Thin Solid Films 669 (2019) 377–386

Contents lists available at ScienceDirect

Thin Solid Films

journal homepage: www.elsevier.com/locate/tsf

Flexible hard TiAlSiN nanocomposite coatings deposited by modulated pulsed power magnetron sputtering with controllable peak power

H. Chen, B.C. Zheng, Y.G. Li, Z.L. Wu, M.K. Lei*

Surface Engineering Laboratory, School of Materials Science and Engineering, Dalian University of Technology, Dalian 116024, China

ARTICLE INFO

Keywords:
Titanium aluminum silicon nitride
Coating
Modulated pulsed power magnetron sputtering
Nanocomposite
Fracture toughness
Flexibility
Hardness

ABSTRACT

TiAlSiN nanocomposite coatings were deposited by modulated pulsed power magnetron sputtering (MPPMS) with the varied peak power from 24.8 to 56.8 kW. The coatings had a typical nc-TiAlN/a-Si_3N_4 nanocomposite structure. The microstructure of the coatings changed from a columnar structure (Zone I in Thornton's Model) at 24.8 kW and 35.2 kW to a dense glassy-like structure (Zone T) at 44.6 kW and 56.8 kW. With increasing peak power from 24.8 to 56.8 kW, the hardness increased from 23.6 to 31.3 GPa, the H/E^* changed from 0.079 to 0.091, elastic recovery (W_e) increased from 50.1% to 57.4%, and compressive macrostress (σ) changed from −0.16 to −1.59 GPa. Fracture toughness (K_{IC}) of the coatings was measured by the indentation test with a Vickers diamond indenter at the load L of 500 mN and 1000 mN. K_{IC} increased from 0.96 to 1.77 MPa·$m^{1/2}$ with the peak power from 24.8 to 44.6 kW, except for no fracture at the highest peak power of 56.8 kW. The highest hardness, H/E^* ratio and elastic recovery of 31.3 GPa, 0.091, 57.4% with the macrostress of −1.59 GPa were obtained at the peak power of 56.8 kW. The enhanced toughness of TiAlSiN nanocomposite coatings was obtained at peak power of 44.6 kW and 56.8 kW, which was attributed to dense structure in the Zone T at high peak power. Effect of the bombarding energy (E_{bi}) and surface mobility (D) of the incident species on Zone T structure was explained by the electron densities and temperature, and number densities of Ti and Al sputtered species simulated using a global plasma model. The critical parameter of structural transformation from a columnar structure to a dense glassy-like structure is the increase of bombarding energy E and mobility of species D. The flexible and hard TiAlSiN nanocomposite coatings were deposited by MPPMS at higher peak power.

1. Introduction

In recent years, TiAlSiN nanocomposite coatings are devoted to development of a new generation of coatings that are used on cutting tools for increasing their lifetime [1,2]. Due to the addition of Si and Al in TiN coatings, TiAlSiN coatings exhibit the enhanced properties, such as high hardness, thermal stability, and oxidation temperature [3,4]. Especially, the Si content in TiAlSiN coatings strongly affects the properties, whose hardness exceeds 50 GPa even though at high temperature [5]. It was reported TiAlSiN coatings were prepared by direct current unbalanced magnetron sputtering (DCMS) [3,6], cathodic arc evaporation (CAE) [7],modulated pulsed power magnetron sputtering (MPPMS) [8], deep oscillation magnetron sputtering (DOMS) [9] and plasma immersion ion deposition [10], which provided excellent mechanical properties. However, the brittleness of the hard TiAlSiN coatings strongly limits their practical utilization. The enhanced toughness is an important task for the TiAlSiN nanocomposite coatings.

The flexible hard nanocomposite coatings represent a new class of coatings, which are simultaneously hard, tough and resistant to cracking [11]. Such coatings should exhibit four essential conditions: (i) a high ratio $H/E^* \geq 0.1$, $E^* = E/(1-\nu^2)$, where E^* is the effective Young's modulus and ν is the Poisson's ratio [12], (ii) the high elastic recovery $W_e \geq 60\%$, (iii) the compressive macrostress $\sigma < 0$, (iv) dense, void-free microstructure which is formed in the transition zone (Zone T) of Thornton's Structure Zone Model (SZM) [13].

The toughness of TiAlSiN coatings is not only correlated with mechanical properties, but also affected by the microstructure of coatings. By traditional preparation process, as like DCMS, CAE and plasma immersion ion deposition, the microstructure of TiAlSiN coatings has a columnar structure in the Zone I of Thornton's SZM with a few open voids in the coatings. The mobility of incident atoms on the surface of the substrate is low, due to the low generated ion energy and ionization rate of DCMS, resulting in a columnar structure. The high-energy large particles during the CAE process increase defect density of the coatings resulting in the deterioration of coating toughness. In the recently years, the new pulsed deposition process has been developed, to acquire

* Corresponding author.
E-mail address: surfeng@dlut.edu.cn (M.K. Lei).

https://doi.org/10.1016/j.tsf.2018.10.031
Received 17 May 2018; Received in revised form 20 October 2018; Accepted 22 October 2018
Available online 24 October 2018

the coatings with dense and void-free microstructure, excellent mechanical and tribological properties [14].

Modulated pulsed power magnetron sputtering (MPPMS), as a variation of high power pulsed magnetron sputtering (HPPMS), shows great potentials advantages comparing with the conventional magnetron sputtering techniques [15]. HPPMS can adjust the ion deposition energy and angle to control the microstructure and properties of the deposited coatings, such as preferred orientation, grain size, coating density and internal stress to achieve uniform deposition on the complex surface using electromagnetic field or substrate bias [16]. MPPMS can produce 10^{18}–10^{19} ions m^{-3} high-density plasma with 80–90% ionization rate by applying high power density and low duty cycle unipolar pulses on the magnetron target and keep the average power lower than the peak power by two orders of magnitude to avoid magnetically controlled targets from overheating [17,18]. The coatings deposited by MPPMS have a smooth surface with a dense and void-free microstructure and a significantly improved quality [19]. In the previous work [8,20], we reported the plasma conditions and the tribological properties of TiAlSiN nanocomposite coatings deposited at the different work pressure and gas ratio of Ar/N_2 by MPPMS. However, the effect of MPPMS pulse shape on the toughness of coatings has not been studied. There is investigated in this work by deposited TiAlSiN coatings and analyzed their properties.

In this paper, TiAlSiN nanocomposite coatings were deposited by MPPMS at varied peak power without the biasing and additional heating. The changes in the toughness of coatings were identified and discussed in the light of the bombarding energy E_{bi} and surface mobility D of the incident species by controlling the peak power.

2. Experimental procedures

TiAlSiN coatings were deposited by MPPMS system that included magnetron sputtering target, vacuum system, power supply, and the work station as illustrated in Fig. 1. Four rectangular magnetron sputtering targets were mounted vertically with a 90° interval, the composition of the hot pressed target was $Ti_{0.47}Al_{0.47}Si_{0.06}$ (99.9% purity), and its size was 440 mm × 140 mm × 6 mm, which was powered at an average power of 1 kW through Zpulser LLC MPPMS power supply. The coatings deposited with the target of this component usually exhibited higher hardness and toughness. The effective sputter area enclosed in

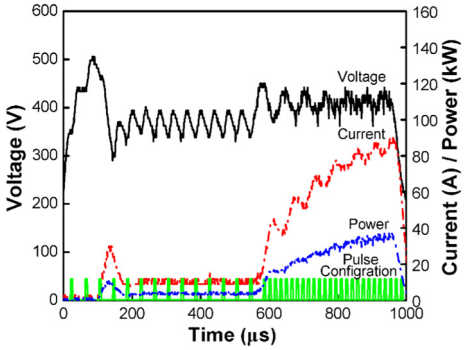

Fig. 2. The typical pulse waveform of MPPMS discharge curve at the peak power of 35.2 kW, including a 600 μs weak ionization stage and a 400 μs strong ionization stage.

the sputter track was 180 cm^2, which was used to calculate the peak power density (P_d) on the target. A base pressure $< 2 \times 10^{-4}$ Pa was obtained before the deposition process, and the working pressure was kept at a constant of 0.5 Pa. The sputtering gas was a mixture of nitrogen and argon with a purity of 99.99%, the total mass flow rate was 80 sccm with the nitrogen partial flow rate of 20%. The deposition temperature was measured by THERMAX surface temperature, which was changed from 195 to 240 °C with increase of the peak power from 24.8 to 56.8 kW. The distance between substrate and target was 100 mm. The Si(100) wafer was used as substrate mounted on substrate holder. There was no additional heat on the substrate as well as bias voltage. The Si(100) substrates were ultrasonically cleaned in alcohol and acetone for 30 min, respectively. Before the MPPMS deposition process, the substrate surface was bombarded for 20 min by using a −350V pulsed DC bias at the working pressure of 2.5 Pa, and the surface of the target was sputtered for 2 min at the pressure of 0.5 Pa, respectively.

Fig. 2 shows an experimental MPPMS pulse waveform at the peak power of 35.2 kW. The macropulse with a length of 1000 μs includes discharge voltage, current, and power, and is consisted of a weak ionization period of 600 μs and a strong ionization period of 400 μs, by manipulating micro-pulse switching times (τ_{on}/τ_{off}). The duty cycle τ_{on}/τ_{off} was 6/34 during the first 600 μs and 6/10 during the last

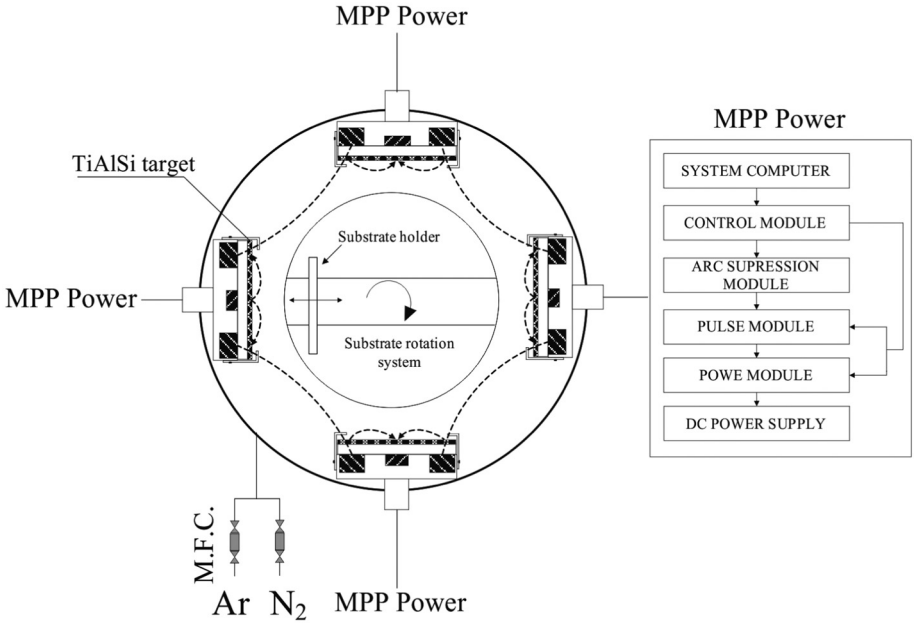

Fig. 1. The schematic structure of four target closed field unbalanced magnetron sputtering system.

Table 1
Deposition pulsing parameters of TiAlSiN coatings by MPPMS at different peak powers.

Sample ID	Pulsing parameters						Deposition conditions						
	τ_{total} [μs]	τ_{weak} [μs]	τ_{on}/τ_{off} [μs]	τ_{strong} [μs]	τ_{on}/τ_{off} [μs]	f [Hz]	P_a [kW]	P_p [kW]	P_d [W/cm^2]	V_p [V]	I_p [A]	Bias [V]	T_s [°C]
C1	1000	600/400	6/34	400	6/10	122	1	24.8	138	401.2	62.2	N/A	195
C2	1000	600/400	6/34	400	6/10	96	1	35.2	196	403.7	87.6	N/A	210
C3	1000	600/400	6/34	400	6/10	75	1	44.6	248	402.4	108.3	N/A	230
C4	1000	600/400	6/34	400	6/10	67	1	56.8	316	408.5	138.2	N/A	245

Note: τ_{total}: total pulse width for one pulse; $\tau_{weak}/\tau_{strong}$: weak and strong ionization periods within one pulse; T_{on}/τ_{off}: voltage off/on times in the weak/strong ionization periods; f: repetition frequency of modulated pulses; P_a and P_p: average and peak powers; P_d: peak power density; V_p and I_p: peak voltage and current; T_s: average substrate temperature with no additional heat.

400 μs. The deposition time for the coatings was 120 min. The detailed pulsing parameters for MPPMS deposition are showed in Table 1.

The chemical composition and the bonding structure of TiAlSiN coatings were analyzed by x-ray photoelectron spectroscopy (XPS), which is an ESCALAB250 system with a monochromatic Al$K\alpha$ x-ray beam at power of 150 W and energy of 1486.5 eV. The charge shift was corrected using a C1s peak with a binding energy of 285.0 eV. The surface of TiAlSiN coating was first subjected to sputter cleaning before XPS testing. The information on the chemical bonding states was achieved by using the XPSPeak software with a mixed Gaussian-Lorentzian product function. For the TiAlSiN coatings on the Si (100) wafer, the crystal structure of coatings was examined by using a monochromatic CuKα radiation on a PANalytical EMPYREAN x-ray diffractometer. The cross-sectional microstructure of the TiAlSiN coatings was examined by using a ZEISS SUPRA-55 VP field emission scanning electron microscope (FESEM). The planar-view microstructure of the TiAlSiN coatings was examined by using a Tecnai 220S-TWIM high resolution transmission electron microscopy (HRTEM). The samples for planar-view HRTEM observation were ground mechanically to a foil with a thickness of about 30 μm. This foil was further thinned down to electron transparency using a Gatan Model 691 precision ion polishing with a 4 keV Ar^+ beam and a 3–7° angle of beam-to-sample surface. HRTEM images were analyzed by Fast Fourier Transform (FFT) method using Gatan digital micrograph software, which provided more structural information in lattice resolution on the microstructure [8]. The hardness H, effective Young's modulus E^* and elastic recovery W_e of the TiAlSiN nanocomposite coatings were measured by a nanoindenter with NanoIndenter XP™, MTS Systems Corporation using a Berkovich diamond tip. The indentation depth was typically 10% of the coating thickness in order to avoid the effect of substrate. By using the Oliver's method, the loading and unloading curves were calculated to obtain the hardness and elastic modulus. At least sixteen valid measurements were made for each sample at a separation distance of 200 μm to obtain statistical results. The macrostress was evaluated from the bending of a thin Si(100) plate by 30 × 5 mm covered by the TiAlSiN coatings using Stoney's formula [21].

The resistance of TiAlSiN coatings to cracking was assessed by the indentation test with a Vickers diamond indenter at loads L of 500 mN and 1000 mN. To avoid influence of the substrate on the result of this test, the load dependent on the coating thickness h must be carefully selected, with the ratio $d/h \leq 0.5$, here d is the penetration depth of the diamond indenter [11]. Failure of the TiAlSiN coatings was expressed by the crack formation from the indent impression, and the fracture toughness K_{IC} of the coatings could be obtained through the following formula [22],

$$K_{IC} = \delta\left(\frac{E}{H}\right)^{1/2}\left(\frac{P}{c^{3/2}}\right) \quad (1)$$

where H and E are the hardness and the elastic modulus of the coatings, c is the length of radial crack, P is the indenter load, and δ is an empirical constant, which depends on the geometry of the indenter. The value of δ is 0.016 for standard Vickers diamond pyramid indenter. The morphologies of Vickers diamond indenter imprint were analyzed by a LEXT 3D measuring laser microscope OLS 4000.

3. Results

3.1. Composition and microstructure

Fig. 3 shows the composition of the TiAlSiN coatings deposited on Si (100) substrate at peak power of 24.8 kW, 35.2 kW, 44.6 kW and 56.8 kW, measured by XPS. A $Ti_{0.20}Al_{0.28}Si_{0.05}N_{0.47}$ coating was detected in the coatings deposited at the peak power of 24.8 kW. With increase of the peak power, the contents of titanium, aluminum, silicon and nitrogen in all TiAlSiN coatings had non obvious change, and the ratio of Al/(Ti + Al) was about 0.58, which is an important factor effecting the structure of coatings [23]. Chen et al. [24] concluded that losses due mainly to the scattering and angular distribution of the sputter flux, together with the different poisoning state of the Ti and Al particles of the powder-metallurgical prepared $Ti_{0.5}Al_{0.5}$ target, led to a huge deviation in the Al/Ti ratio of the films as compared to the target. No change in the average power of 1 kW led to the similar composition of TiAlSiN coatings at the changed peak power from 24.6 to 56.8 kW.

Fig. 4 shows the XRD patterns of the TiAlSiN coatings deposited at the peak power of 24.8–56.8 kW. All of the TiAlSiN coatings had c-TiAlN(111), (200), (220) and (311) diffraction peaks. With increasing the peak power, the intensity of (200) and (311) peaks of c-TiAlN became strong, while the (111) peak slightly decreased. For transition metal nitrides, more intense energetic bombardment has enhanced surface diffusion, the adatoms will be accommodated in the (200) planes which exhibit a lower surface free energy than that of the (111) planes [25].

Fig. 5 shows the cross-sectional SEM micrographs of the TiAlSiN coatings at the peak power of 24.8–56.8 kW. The thickness of TiAlSiN coatings decreased from 2.6 to 2.1 μm, leading to deposition rate (α_D) of the coatings decrease from 21.6 to 17.5 nm/min with increasing the

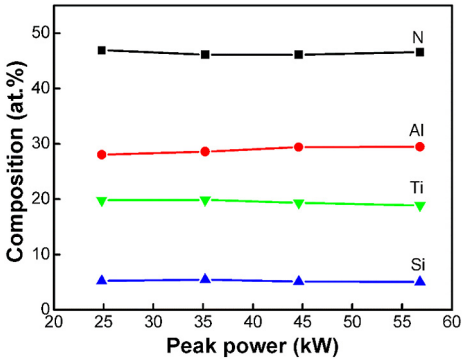

Fig. 3. The composition of TiAlSiN coatings deposited by MPPMS at different peak powers.

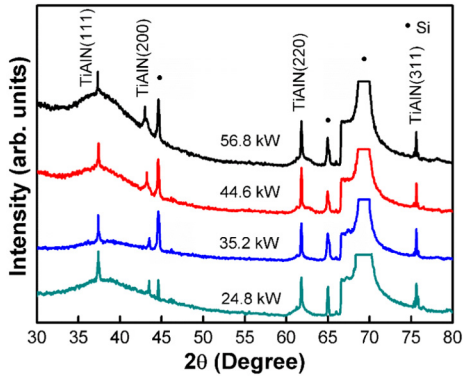

Fig. 4. The XRD patterns of TiAlSiN coatings deposited by MPPMS at different peak powers.

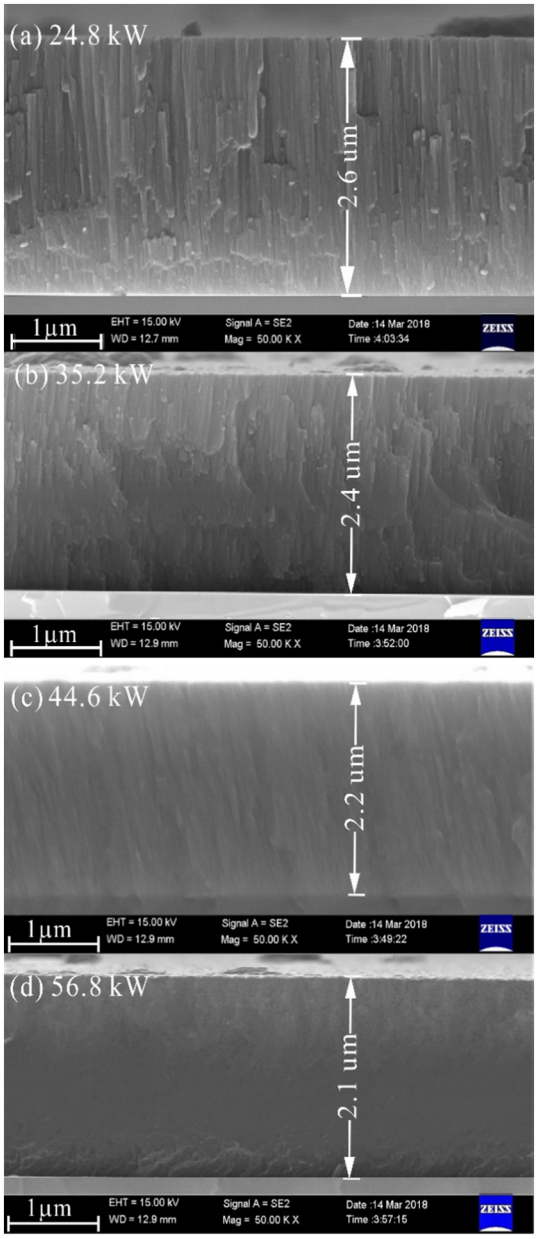

Fig. 5. The cross-sectional SEM images of TiAlSiN coatings deposited by MPPMS at different peak powers.

peak power. The decrease of deposition rate with increase of peak current/power density corresponds well to the literature for MPPMS discharges [26], due to redirect the metal ions to the target for re-sputtering or sideway transport. All the TiAlSiN coatings exhibited dense and voids-free microstructure. An obvious columnar morphology in the Zone I of SZM could be seen in the TiAlSiN coatings deposited at the peak powers of 24.8 kW and 35.2 kW, whereas a glassy like structure in the Zone T was detected at the peak power of 44.6 kW and 56.8 kW. The microstructure of the TiAlSiN coatings changed from dense columnar in the Zone I to glassy like structure in the Zone T with high peak power. A similar result was reported that the structure of CrN coatings changed from the Zone I to the Zone T with the increase of peak power by HIPIMS [27].

Fig. 6 shows the planar-view TEM images of the TiAlSiN coatings deposited at the peak power of 24.8 kW and 44.6 kW. The selected area diffraction SAD patterns in the two coatings indicated a polycrystalline TiAlN phase was generated, and c-TiAlN(111), (200), (220), (222) and (311) reflections were identified, which was in agreement with the XRD results. The TEM microstructure of the coatings was dense with no voids. From the HRTEM images of the TiAlSiN coatings, there was a typical nanocomposite structure consisting of nanocrystalline TiAlN embedded in an amorphous matrix Si_3N_4. The TiAlN grain size was around 8–10 nm at 24.8 kW and 5–6 nm at 44.6 kW, as well as the width of amorphous phase was around 2–3 nm in the two TiAlSiN coatings. When the ratio of grain size to width of amorphous phase is close to 1, the toughness of the nanocomposite coatings will be significantly enhanced [28].

Fig. 7 shows the XPS spectra of the TiAlSiN coatings deposited at a peak power of 24.6–56.8 kW in Ti2p, Al2p, Si2p and N1 s binding energy regions, respectively. The deconvolution of the Ti2p peak displayed that it was composed of three peaks centered at the binding energy values of 455.4 eV, 456.7 eV and 457.9 eV, indicating that titanium in the coating represented as TiN, titanium oxynitride and Ti_2O_3 [29]. For the Al2p spectra, a single peak at the binding energy of 74.4 eV was detected in all of the coatings, which was assigned to AlN phase [6]. In the Si2p spectra, the binding energy of Si2p peak centered at 102.1 eV was associated with Si_3N_4 [10]. The N1 s spectra of the coatings showed the presence of two peaks at 397.1 eV and 398.2 eV [8]. The high intensity peaks of 397.1 eV was assigned to TiAlN bonds. Because the binding energy of pure TiN and AlN is 396.7 eV and 397.3 eV, the observed peak shift may be attributed to the change of bonding structure in TiN crystallites by incorporation of Al atoms, which was consistent with the XRD results. The low intensity peak located at 398.2 eV indicated the formation of Si_3N_4. It could be concluded that Si_3N_4 was in an amorphous state in the TiAlSiN coatings, the coatings had a nc-TiAlN/a-Si_3N_4 nanocomposite structure denoted by XRD, TEM and XPS.

3.2. Mechanical property and residual stress

Table 2 shows the hardness (H), effective elastic modulus (E^*), ratio H/E^*, elastic recovery (W_e) values, and residual stress (σ) of the TiAlSiN nanocomposite coatings deposited on Si(100) substrate at the peak power of 24.8–56.8 kW. With increasing the peak power, the hardness had a linear increase from 23.6 to 31.6 GPa, and H/E^* value increased from 0.075 to 0.091, the same as W_e value from 50.1% to 57.4%. At the peak power of 56.8 kW, the TiAlSiN nanocomposite coating has highest hardness, ratio H/E^*, and elastic recovery of 31.3 GPa, 0.091, and 57.4%, respectively. The residual compressive stress of the TiAlSiN nanocomposite coating raised from −0.16 GPa to −1.59 GPa with increase in the peak power from 24.8 to 56.8 kW. The change of mechanical properties was mainly due to the microstructure evolution of the TiAlSiN coatings from the Zone I to the Zone T as shown in Fig. 3. Recently, the ratios H/E^* and W_e were recognized as the indicators of the toughness of coatings [11]. The hardness of the TiAlSiN nanocomposite coating should be high enough to provide resistance to

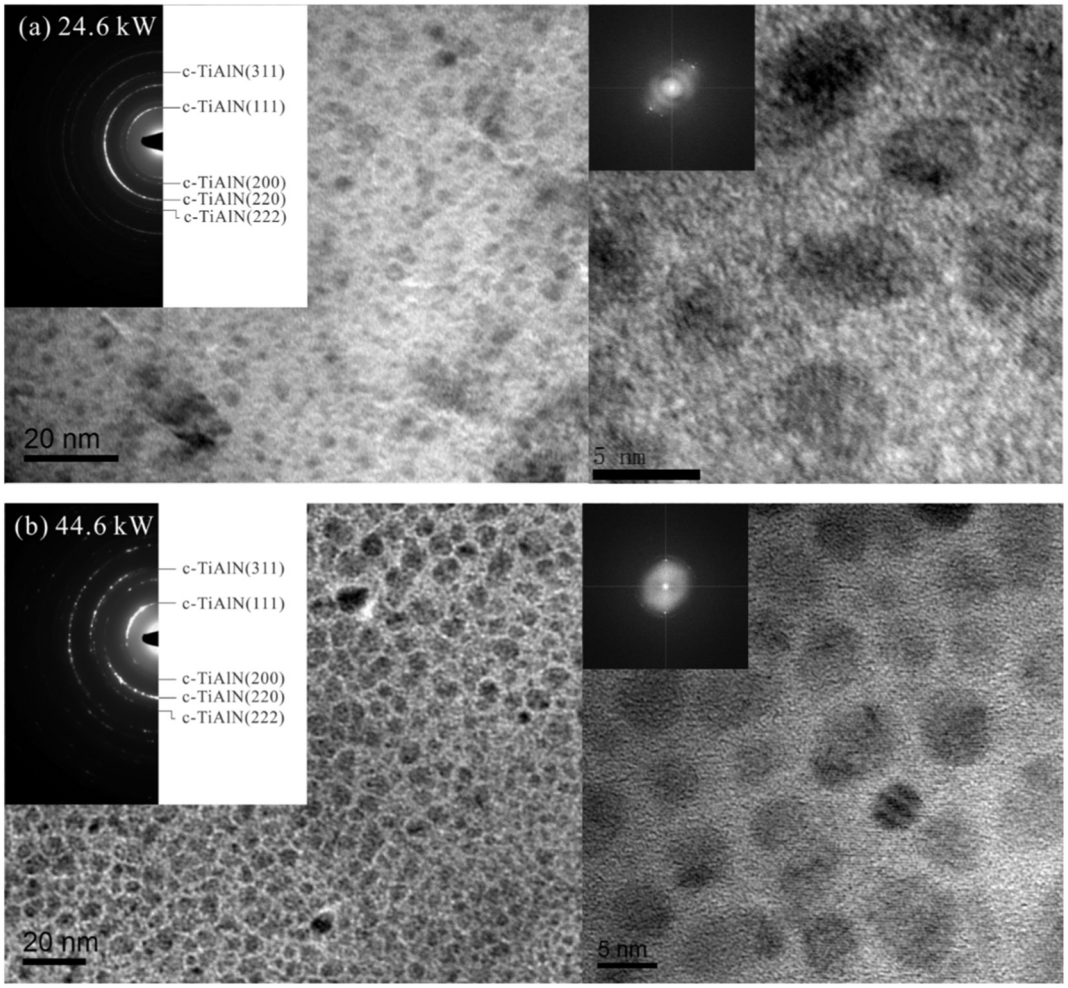

Fig. 6. The planar view HRTEM images of TiAlSiN coatings deposited by MPPMS at different peak powers.

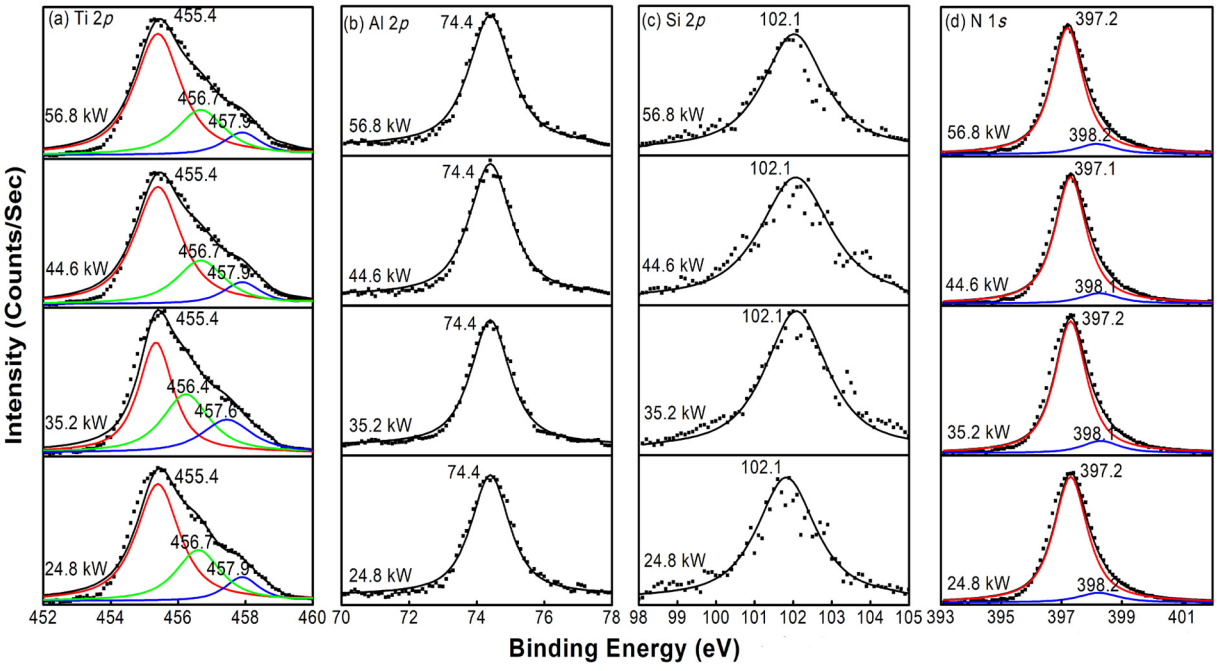

Fig. 7. The XPS core level spectra of TiAlSiN coatings deposited by MPPMS: (a) Ti2p, (b) Al2p, (c) Si2p, and (d) N1s.

Table 2
Mechanical property and residual stress of TiAlSiN coatings by MPPMS at different peak powers.

P_p [kW]	H [GPa]	E^* [GPa]	H/E^*	W_e [%]	σ [GPa]
24.8	23.6	312.5	0.075	50.1	−0.16
35.2	25.9	321.7	0.081	53.2	−0.29
44.6	27.5	326.1	0.084	54.8	−0.72
56.8	31.6	346.2	0.091	57.4	−1.59

Note: P_p – peak power; H and E^* – hardness and effective elastic modulus; W_e – elastic recovery; σ – residual stress.

plastic deformation, while low values of effective Young's modulus are desirable in order to distribute the load applied to the coating over a wider area.

3.3. Fracture toughness

Fig. 8 shows the surface morphology of the indentation test with a diamond impression at the loads L of 500 mN and 1000 mN, respectively, on the TiAlSiN nanocomposite coatings deposited at the peak power from 24.8 to 56.8 kW, observed by laser scanning confocal microscope. At the load of 500 mN, the ratio d/h decreased from 0.5 to 0.43 with increase of the peak power. At the peak power of 24.8 kW and 35.2 kW, the length of cracks was 9.61 μm and 9.01 μm, and the fracture toughness K_{IC} of the coatings was 0.95 MPa·$m^{1/2}$ and 1.01 MPa·$m^{1/2}$, respectively, according to the Formula (1). There was no crack on the coatings at the peak power of 44.6 kW and 56.8 kW, which indicated that the toughness of coatings was improved. At the load 1000 mN, the ratio d/h decreased from 0.73 to 0.61 with the higher peak power, indicating that the indentation was affected by the substrate at the high load. When the peak power increased from 24.8 to 44.6 kW, the length of cracks decreased from 15.13 to 9.72 μm, K_{IC} increased from 0.96 to 1.77 MPa·$m^{1/2}$. There was no crack in the TiAlSiN coating at the peak power of 56.8 kW, even though d/h was above 0.5. It was shown that the TiAlSiN nanocomposite coating deposited at the peak power 56.8 kW had high hardness and good toughness. More details are shown in Table 3. A similar result was reported by Nakonechna et al. [30] that the 2 μm thick TiAlSiN coatings with the hardness of 29–32.5 GPa had a fracture toughness of 1.55–2.1 MPa·$m^{1/2}$.

4. Discussion

4.1. Effect of MPPMS plasma on microstructure of TiAlSiN nanocomposite coatings

From toughness tests, the TiAlSiN nanocomposite coatings with a Zone T structure exhibited an enhanced toughness. The influence of the plasma parameters during a MPPMS pulse on the microstructure of the TiAlSiN coatings was simulated by a spatially averaged, time-dependent global plasma model [20,31]. The model was used to describe the TiAlSiN nanocomposite coatings deposited by reactive MPPMS discharges in Ar/N_2 mixture gas, based on the energy balance and the particle balance in the ionization region, and considering the formation and erosion of the compound at the target surface. The introduction of reactive gas species was considered as well, which increased the

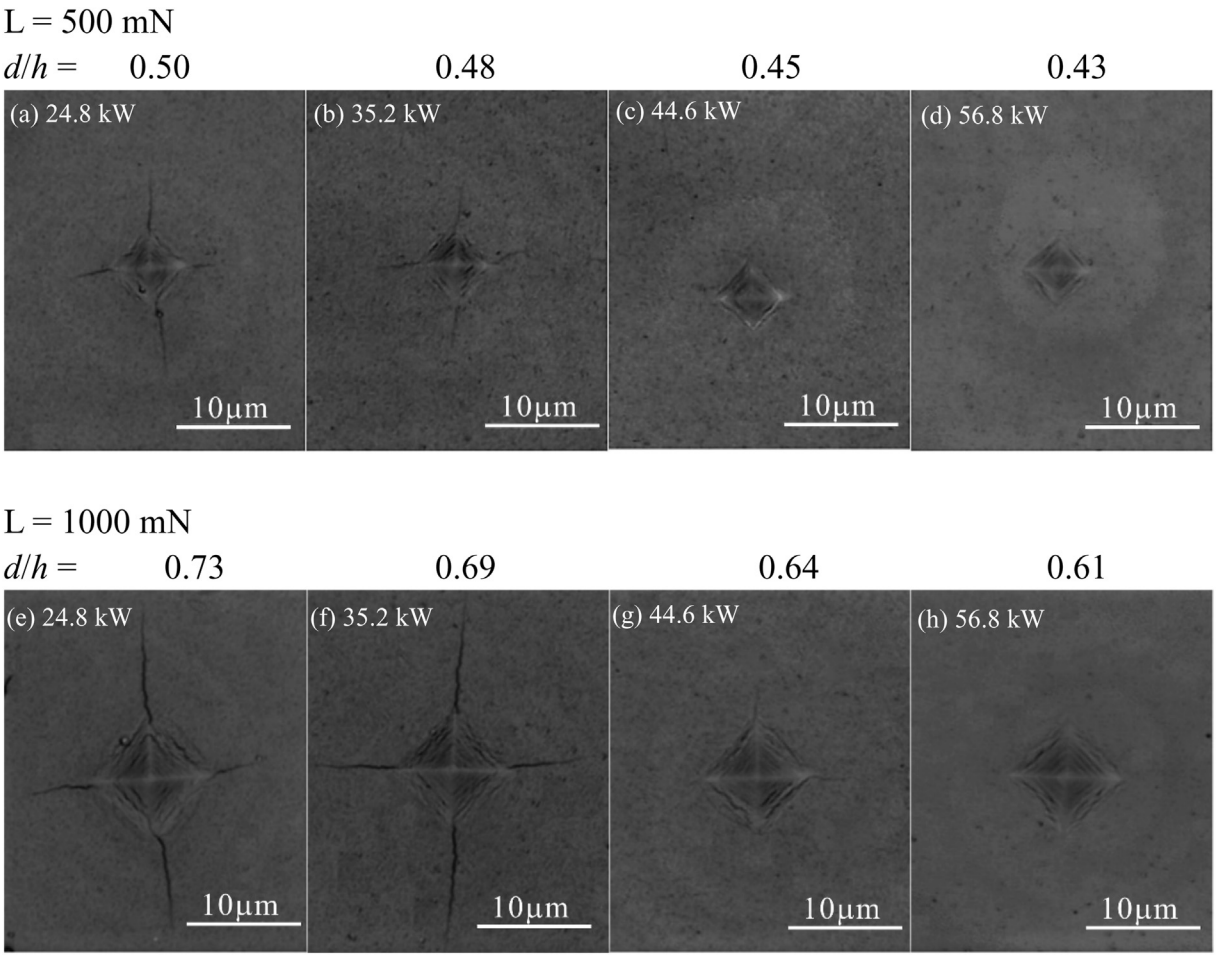

Fig. 8. The Photos of indentation impressions under the loads of 500 mN and 1000 mN into the surface of the TiAlSiN nanocomposite coatings deposited at different peak powers.

Table 3
The results of indentation test under the loads of 500 mN and 1000 mN into the surface of the TiAlSiN nanocomposite coatings deposited at different peak power.

P_p [kW]	h [μm]	L = 500 mN					L = 1000 mN				
		d_1 [μm]	d_1/h	c_1 [μm]	K_{IC} [MPa·m$^{1/2}$]	Cracks	d_2 [μm]	d_2/h	c_2 [μm]	K_{IC} [MPa·m$^{1/2}$]	Cracks
24.8	2.6	1.26	0.50	9.61	0.946	Yes	1.73	0.73	15.13	0.958	Yes
35.2	2.4	1.19	0.48	9.01	1.013	Yes	1.6	0.69	14.51	0.989	Yes
44.6	2.2	0.99	0.45	–	–	No	1.42	0.64	9.72	1.769	Yes
56.8	2.1	0.90	0.43	–	–	No	1.24	0.61	–	–	No

Note: P_p – peak power; h and d – film thickness and indentation depth; c – the length of crack; K_{IC} – the fracture toughness.

complexity of MPPMS discharges. The reactive MPPMS model was an extension of the previous MPPMS discharge model, and the numerical procedure was the same as the previous one except that the Hall parameter $\omega_{ge}\tau_c$ was fitted time-dependently, which improves the fitting accuracy during the entire macropulse. By fitting the global model to duplicate the experimental discharge currents on the different MPPMS conditions, the plasma parameters, such as the densities of each species sputtered and the electron temperature T_e, were obtained to describe the deposition dynamics.

During the sputtering process, the average power and the working pressure as well as the nitrogen partial pressure ratio were fixed, they were 1 kW, 0.5 Pa and 25%, respectively, only peak power was changed from 24.6 to 56.8 kW. The experimental discharge voltage and current were used as the input parameters, then the MPPMS discharge process was simulated by the global plasma model, the specific parameters of the plasma during the discharge process could be achieved. Fig. 9 shows the electron densities and temperatures in a macropulse with a length of 1000 μs at the peak power of 24.8–56.8 kW. The electron densities n_e at the peak powers were obtained between 1.1×10^{18} ions m^{-3} and 1.4×10^{18} ions m^{-3} in the weak ionization period of the first 600 μs, and then increased rapidly in the strong ionization period of the 400 μs

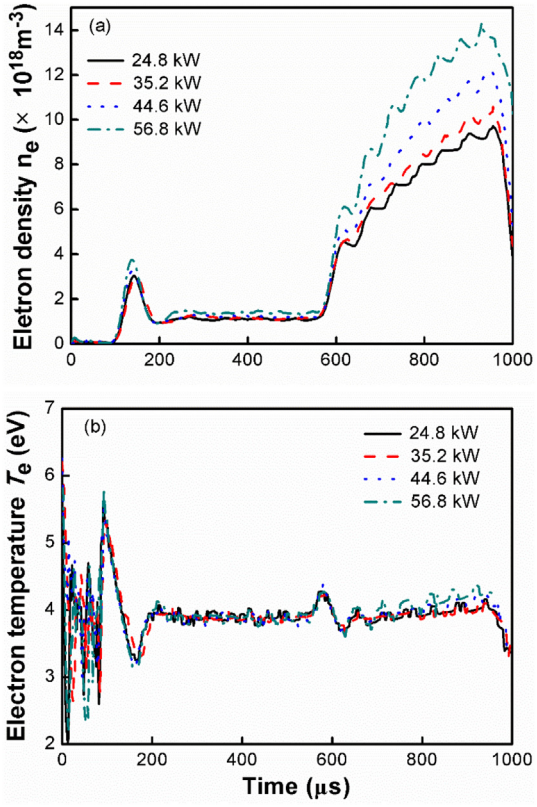

Fig. 9. Electron densities and temperature calculated by global plasma model at the different peak powers.

to 9.2×10^{18} ions m^{-3} and 14.2×10^{18} ions m^{-3}. The electron temperature T_e was kept at as a constant of 4 eV, since the energy loss of electrons due to collisions was similar at a fixed working pressure during the MPPMS discharge. Fig. 10 shows the densities of Ti and Al species sputtered in a macropulse with a length of 1000 μs at the peak power of 24.8–56.8 kW. The sputtered species were sputtered atoms and ions of Ti, Al, Si, the Al and Ti species were dominant, especially the Al^+ and Ti^+ ions with the similar densities, in the strongly ionized region between 9.5×10^{17} ions m^{-3} and 14.5×10^{17} ions m^{-3}. The density of the Si species was too little compared with the Al^+ and Ti^+ species, as 1×10^{17} ions m^{-3}. It can be seen that, with an increase of the peak power from 24.8 to 56.8 kW during a MPPMS pulse, the densities of species sputtered calculated from the integrated area increased by 40%. Meanwhile, the ionization rates of species sputtered increased from 65% to 80%.

The energy E_{bi} of bombarding species delivered to the growing coating has very important effect on the microstructure, phase composition and mechanical properties. The E_{bi} could be expressed by the following formula [32],

$$E_{bi} \approx U_s i_s / a_D \quad (2)$$

where U_s is the substrate bias, and i_s is the substrate current, a_D is deposition rate. Since there was no negative bias in the deposition process, U_s is a floating potential U_f that is established on the substrate and accelerates the arriving ions, and could be derived as $U_f = -T_e \ln(M/2\pi m)^{1/2}$. T_e is electron temperature, M and m are the mass of the ion and the electron, respectively [20]. U_f is around 31 V at all the peak powers, i_s is proportional to the ionization rates of species sputtered, a_D is from 21.6 to 17.5 nm/min with increasing of the peak power. E_{bi} at peak power of 56.8 kW is larger by 45% than that at 24.8 kW. With an increase in E_{bi}, the microstructure changed from columnar structure in the Zone I to dense structure in the Zone T. Musil [33] reported the same behaviors for the TiN coatings during magnetron sputtering deposition with the E_{bi} toward the coatings.

The both neutral and ionized species reaching onto the substrate in the MPPMS pulse also affected the microstructural evolution of coatings, as the density of island nucleation and surface mobility of the incident species. The higher density of island nucleation which was effected by the density of species sputtered could enhance the formation of continuous film. The surface mobility D can be expressed by the following formula [34],

$$D = \frac{1}{4} l^2 \nu_0 \exp\left(-\frac{E_D}{k_B T}\right) \quad (3)$$

where l for simplicity, ν_0 is an attempt frequency, E_D is the energy barrier of surface mobility. The deposition temperature T was changed from 195 to 240 °C with an increase of the peak powers from 24.8 to 56.8 kW. From Formula (3), the surface mobility of incident species D at the peak power of 56.8 kW was 1.7 times larger than that at 24.8 kW. When the surface mobility of the incident species at the peak power of 24.8 kW was very low, the species arrived at coating surface and remained at their arrival position, which led to the rough surface topography of coatings during coarsening process. As a result, the stabilized

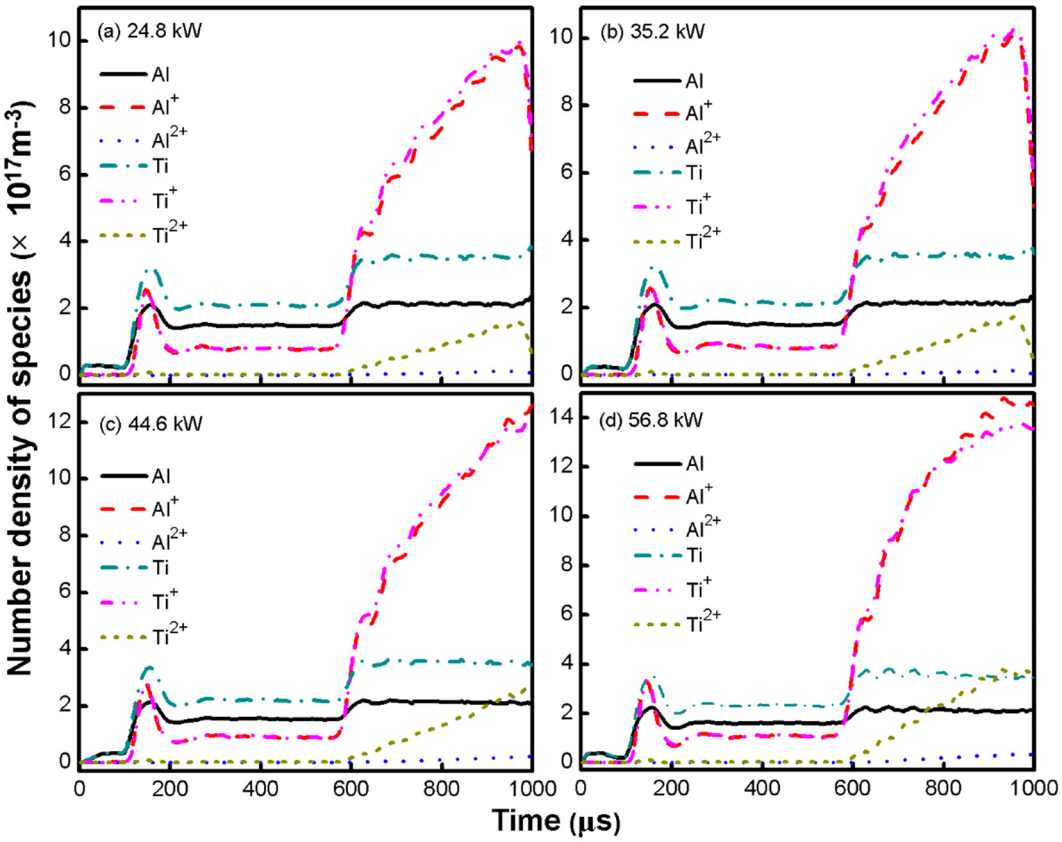

Fig. 10. Densities of Ti and Al sputtered species calculated by global plasma model at the different peak powers.

roughness can create a columnar growth mode with columnar structure [35]. If the species sputtered reached on the coating surface at a range of angles rather than a normal angle, the shadowing effects carried out on the surface, resulted by competitive growth of columns with the structure in the Zone I and by replacement of the grain boundaries using the voids or walls of low density.

The TiAlSiN nanocomposite coatings were deposited by MPPMS with a peak power controlled from 24.8 to 56.8 kW. The microstructure of the TiAlSiN coatings was changed from a columnar structure in the Zone I to a dense and voids-free structure in the Zone T by increasing the bombarding energy E_{bi} and the surface mobility of incident species D at the MPPMS conditions, although the kinetic roughening and shadowing effects depended on the microstructure of the Zone I. Generally, the Zone T structure was formed at the ratio of substrate temperature and melting temperature of coating material (T_s/T_m) about 0.3 to 0.5 and/or with high kinetic energy of incident species [13,36]. The elevated deposition temperature is usually obtained by additional heating and energetic species bombardment at lower pressure or higher negative bias. There are no additional heating and the biasing in the MPPMS, the bombarding energy E_{bi} and incident species mobility D can be increased by modulating the peak power, which lead to the formation of a Zone T structure of the TiAlSiN nanocomposite coatings.

4.2. Toughness of TiAlSiN nanocomposite coatings

From the indentation test of the TiAlSiN nanocomposite coatings deposited at the different peak powers, the coatings at the peak powers of 44.6 kW and 56.8 kW were obtained as flexible and hard coatings. Fig. 11 shows the formation conditions of the hard and tough properties of the TiAlSiN nanocomposite coatings deposited by MPPMS. It could be seen that the TiAlSiN nanocomposite coatings with a dense and void-free structure in the Zone T exhibited an enhanced resistance to cracking, when the peak power was above 44.6 kW. The fracture toughness K_{IC} of the TiAlSiN nanocomposite coatings increased with high peak power. H/E^* represents the ability of the coating resistance against elastic strain to failure. H/E^* is directly related to the deformation of the material ε in the indentation test [37],

$$\sigma = E \cdot \varepsilon \tag{4}$$

$$\sigma_y = \frac{B^n}{3} H \tag{5}$$

where $\varepsilon = \frac{H}{E^*} \cdot \frac{B^n}{3(1-\nu^2)}$, σ_y is yield stress of coatings, B is a constant of 0.1, and n is a hardening index of 0.3. The larger of H/E^*, the greater of the elastic strain ε. W_e represents the ability of the elastic recovery of the coating after compression. With increasing the H/E^*, W_e and K_{IC} in the TiAlSiN nanocomposite coatings, the resistance to elastic and plastic deformation increased.

The TiAlSiN nanocomposite coatings had a columnar structure in the Zone I with visible columnar boundaries at the peak powers of 24.8 kW and 35.2 kW, however, a dense and void-free microstructure in the Zone T at the peak powers of 44.6 kW and 56.8 kW. The TiAlSiN nanocomposite coatings at the peak powers of 24.8 kW and 35.2 kW were easy to crack through the columnar boundaries. There was no columnar boundary in the TiAlSiN nanocomposite coatings at the peak powers of 44.6 kW and 56.8 kW to neglect the cracking. Pei et al. [28,38] reported that the columnar boundary of the nanocomposite coatings was a potential source of failure for loading and contacting sliding. Since the homogeneity of the nanocomposite was interrupted by the columnar boundary, the columnar boundary can serve as the starting position for the crack and the preferred cracking path. Therefore, the enhanced toughness of the TiAlSiN nanocomposite coatings is attributed to the dense and voids-free structure in the Zone T with the excellent mechanical properties.

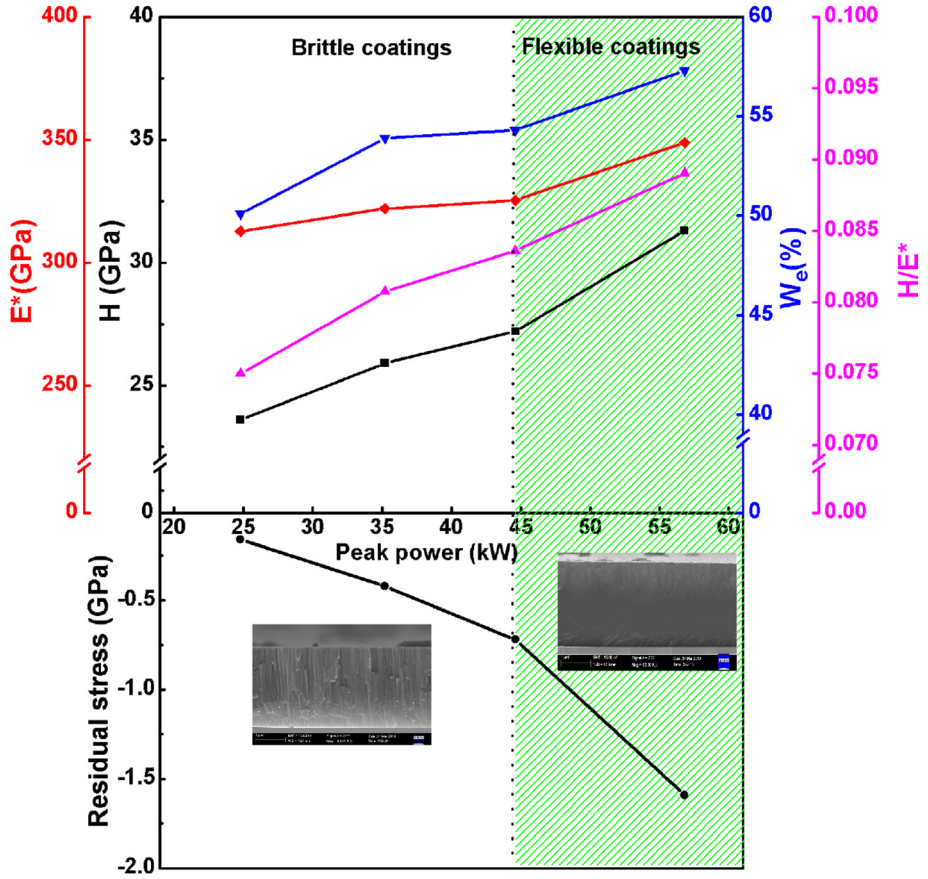

Fig. 11. The formation condition of the hard and tough properties of the TiAlSiN nanocomposite coatings deposited by MPPMS at different peak powers.

5. Conclusions

TiAlSiN nanocomposite coatings were deposited by MPPMS at a peak power of 24.8–56.8 kW, the composition of the coatings was kept at a constant of $Ti_{0.20}Al_{0.28}Si_{0.05}N_{0.47}$. The microstructure of the coatings with a typical nanocomposite structure consisting of nanocrystalline TiAlN embedded in an amorphous matrix Si_3N_4 was changed from a columnar structure in the Zone I to a dense glassy-like structure in the Zone T. With increasing the peak power from 24.8 to 56.8 kW, the TiAlSiN nanocomposite coatings had the hardness changed from 23.6 to 31.3 GPa, the H/E^* ratio from 0.079 to 0.091, the elastic recovery W_e from 50.1% to 57.4%, and the compressive macrostress σ from −0.16 to −1.59 GPa. The fracture toughness K_{IC} of the coatings increased from 0.96 to 1.77 MPa·$m^{1/2}$ with the peak powers of 24.8–44.6 kW. Effect of the bombarding energy E_{bi} and surface mobility D of the incident species in MPPMS deposition process on the Zone T structure was explained by the electron densities and temperature, and number densities of Ti and Al sputtered species simulated using a global plasma model. The bombarding energy E_{bi} was calculated based on the floating voltage and the ionization rates. The surface mobility of incident species D was at the deposition temperature resulted by the bombarding energy E_{bi}. The enhanced toughness of TiAlSiN nanocomposite coatings was depended on the dense and voids-free structure in the Zone T with excellent mechanical properties. The TiAlSiN nanocomposite coatings at the peak powers of 44.6 kW and 56.8 kW were obtained as flexible hard ones, whereas the other TiAlSiN coatings at the peak powers of 24.8 kW and 35.2 kW were brittle ones.

Acknowledgments

The authors thank valuable and helpful discussion of Professor J. Musil, and technical assistance of PhD. students S. Tong and H. L. Che in this paper. This work is supported by National Natural Science Foundation of China under Grants No. 51575077 and 51601029 and the Foundation for Innovative Research Groups of the National Natural Science Foundation of China under Grants No. 51621064.

References

[1] J.S. Kim, G.J. Kim, M.C. Kang, J.W. Kim, K.H. Kim, Cutting performance of Ti-Al-Si-N-coated tool by a hybrid-coating system for high-hardened materials, Surf. Coat. Technol. 193 (2005) 249–254.
[2] Y.Y. Chang, H.M. Lai, Wear behavior and cutting performance of CrAlSiN and TiAlSiN hard coatings on cemented carbide cutting tools for Ti alloys, Surf. Coat. Technol. 259 ((2014) 152–158.
[3] D. Philippon, V. Godinho, P.M. Nagy, M.P. Delplancke-Ogletree, A. Fernández, Endurance of TiAlSiN coatings: effect of Si and bias on wear and adhesion, Wear 270 (2011) 541–549.
[4] A. Miletić, P. Panjan, B. Škorić, M. Čekada, G. Dražič, J. Kovač, Microstructure and mechanical properties of nanostructured Ti-Al-Si-N coatings deposited by magnetron sputtering, Surf. Coat. Technol. 241 (2014) 105–111.
[5] P. Holubář, M. Jílek, M. Šíma, Nanocomposite nc-TiAlSiN and nc-TiN-BN coatings: their applications on substrates made of cemented carbide and results of cutting tests, Surf. Coat. Technol. 120–121 (1999) 184–188.
[6] H.C. Barshilia, M. Ghosh, R. Shashidhara, K.S. Rajam Ramakrishna, Deposition and characterization of TiAlSiN nanocomposite coatings prepared by reactive pulsed direct current unbalanced magnetron sputtering, Appl. Surf. Sci. 256 (2010) 6420–6426.
[7] G.G. Fuentes, E. Almandoz, R. Pierrugues, R. Martínez, R.J. Rodríguez, J. Caro, M. Vilaseca, High temperature tribological characterisation of TiAlSiN coatings produced by cathodic arc evaporation, Surf. Coat. Technol. 205 (2010) 1368–1373.
[8] Z.L. Wu, Y.G. Li, B. Wu, M.K. Lei, Effect of microstructure on mechanical and tribological properties of TiAlSiN nanocomposite coatings deposited by modulated pulsed power magnetron sputtering, Thin Solid Films 597 (2015) 197–205.
[9] Y.X. Ou, H.C.Z.Y. Li, J.L.W. Pan, M.K. Lei, Microstructure and tribological behavior of TiAlSiN coatings deposited by deep oscillation magnetron sputtering, J. Am. Ceram. Soc. 101 (2018) 5166–5176.
[10] T. Chen, Z. Xie, F. Gong, Z. Luo, Z. Yang, Correlation between microstructure evolution and high temperature properties of TiAlSiN hard coatings with different Si and Al content, Appl. Surf. Sci. 314 (2014) 735–745.

[11] J. Musil, Advanced hard coatings with enhanced toughness and resistance to cracking, Chapter 7 in the Book, in: S. Zhang (Ed.), Thin Films and Coatings. Toughening and Toughness Characterization, CRC Press, USA, 2015, pp. 377–464.
[12] J. Musil, Flexible hard nanocomposite coatings, RSC Adv. 5 (2015) 60482–60495.
[13] J.A. Thornton, High rate thick film growth, Annu. Rev. Mater. Sci. 7 (1977) 239–260.
[14] Y.X. Ou, J. Lin, S. Tong, H.L. Che, W.D. Sproul, M.K. Lei, Wear and corrosion resistance of CrN/TiN superlattice coatings deposited by a combined deep oscillation magnetron sputtering and pulsed dc magnetron sputtering, Appl. Surf. Sci. 351 (2015) 332–343.
[15] J. Lin, W.D. Sproul, J.J. Moore, Z. Wu, S. Lee, R. Chistyakov, B. Abraham, Recent advances in modulated pulsed power magnetron sputtering for surface engineering, JOM 63 (2011) 48–58.
[16] A. Anders, J. Andersson, A. Ehiasarian, High power impulse magnetron sputtering: Current-voltage-time characteristics indicate the onset of sustained self-sputtering, J. Appl. Phys. 102 (2007) 113303.
[17] J. Alami, K. Sarakinos, G. Mark, M. Wuttig, On the deposition rate in a high power pulsed magnetron sputtering discharge, Appl. Phys. Lett. 89 (2006) 154104.
[18] A.P. Ehiasarian, A. Hecimovic, T. De Los Arcos, R. New, V. Schulz-Von Der, M. Gathen, J. Winter Boke, High power impulse magnetron sputtering discharges: Instabilities and plasma self-organization, Appl. Phys. Lett. 100 (2012) 114101.
[19] M. Samuelsson, D. Lundin, J. Jensen, M.A. Raadu, J.T. Gudmundsson, U. Helmersson, On the film density using high power impulse magnetron sputtering, Surf. Coat. Technol. 205 (2010) 591–596.
[20] B.C. Zheng, Z.L. Wu, B. Wu, Y.G. Li, M.K. Lei, A global plasma model for reactive deposition of compound films by modulated pulsed power magnetron sputtering discharges, J. Appl. Phys. 121 (2017) 171901.
[21] J. Musil, M. Šašek, P. Zeman, R. Čerstvý, D. Heřman, J.G. Han, V. Šatava, Properties of magnetron sputtered Al-Si-N thin films with a low and high Si content, Surf. Coat. Technol. 202 (2008) 3485–3493.
[22] D.B. Marshall, B.R. Lawn, A.G. Evans, Elastic/plastic indentation damage in ceramics: the lateral crack system, J. Am. Ceram. Soc. 65 (1982) 561–566.
[23] Y. Pinot, M.J. Pac, P. Henry, C. Rousselot, Y.I. Odarchenko, D.A. Ivanov, C. Ulhaq-Bouillet, O. Ersen, M.H. Tuilier, Friction behaviour of TiAlN films around cubic/hexagonal transition: a 2D grazing incidence X-ray diffraction and electron energy loss spectroscopy study, Thin Solid Films 577 (2015) 74–81.
[24] L. Chen, M. Moser, Y. Du, P.H. Mayrhofer, Compositional and structural evolution of sputtered Ti-Al-N, Thin Solid Films 517 (2009) 6635–6641.
[25] P. Patsalas, C. Gravalidis, S. Logothetidis, Surface kinetics and subplantation phenomena affecting the texture, morphology, stress, and growth evolution of titanium nitride films, J. Appl. Phys. 96 (2004) 6234–6235.
[26] F. Papa, H. Gerdes, R. Bandorf, A.P. Ehiasarian, I. Kolev, G. Braeuer, R. Tietema, T. Krug, Deposition rate characteristics for steady state high power impulse magnetron sputtering (HIPIMS) discharges generated with a modulated pulsed power (MPP) generator, Thin Solid Films 520 (2011) 1559–1563.
[27] J. Alami, K. Sarakinos, F. Uslu, M. Wuttig, On the relationship between the peak target current and the morphology of chromium nitride thin films deposited by reactive high power pulsed magnetron sputtering, J. Phys. D. Appl. Phys. 42 (2008) 015304.
[28] Y.T. Pei, D. Galvan, J.T.M. De Hosson, Nanostructure and properties of TiC/a-C:H composite coatings, Acta Mater. 53 (2005) 4505–4521.
[29] P.W. Shum, Z.F. Zhou, K.Y. Li, Y.G. Shen, XPS, AFM and nanoindentation studies of $Ti_{1-x}Al_xN$ films synthesized by reactive unbalanced magnetron sputtering, Mater. Sci. Eng. B 100 (2003) 204–213.
[30] O. Nakonechna, T. Cselle, M. Morstein, A. Karimi, On the behaviour of indentation fracture in TiAlSiN hard thin films, Thin Solid Films 447–448 (2004) 406–412.
[31] B.C. Zheng, D. Meng, H.L. Che, M.K. Lei, On the pressure effect in energetic deposition of Cu thin films by modulated pulsed power magnetron sputtering: a global plasma model and experiments, J. Appl. Phys. 117 (2015) 203302.
[32] H. Poláková, J. Musil, J. Vlček, J. Allaart, C. Mitterer, Structure-hardness relations in sputtered Ti-Al-V-N films, Thin Solid Films 444 (2003) 189–198.
[33] J. Musil, V. Poulek, V. Valvoda, R. Kužel, H.A. Jehn, M.E. Baumgärtner, Relation of deposition conditions of Ti-N films prepared by d.c. magnetron sputtering to their microstructure and macrostress, Surf. Coat. Technol. 60 (1993) 484–488.
[34] D. Magnfält, V. Elofsson, G. Abadias, U. Helmersson, K. Sarakinos, Time-domain and energetic bombardment effects on the nucleation and coalescence of thin metal films on amorphous substrates, J. Phys. D. Appl. Phys. 46 (2013) 215303.
[35] C.V. Thompson, Structure evolution during processing of polycrystalline films, Annu. Rev. Mater. Sci. 30 (2000) 159–190.
[36] A. Anders, A structure zone diagram including plasma-based deposition and ion etching, Thin Solid Films 518 (2010) 4087–4090.
[37] J.R. Cahoon, W.H. Broughton, A.R. Kutzak, The determination of yield strength from hardness measurements, Metall. Trans. 2 (1971) 1979–1983.
[38] D. Galvan, Y.T. Pei, J.T.M. De Hosson, Deformation and failure mechanism of nanocomposite coatings under nano-indentation, Surf. Coat. Technol. 200 (2006) 6718–6726.